September 17, 2014

Rapid Decline of Lyman-α Emission Toward the Reionization Era

V. Tilvi
C. Papovich
H.C. Ferguson
S.L. Finkelstein
J. Long, et al.

Preprint typeset using LaTeX style emulateapj v. 5/2/11

RAPID DECLINE OF LYMAN-α EMISSION TOWARD THE REIONIZATION ERA

V. Tilvi [1], C. Papovich[1], S. L. Finkelstein[2], J. Long[3], M. Song[2], M. Dickinson [4], H. C. Ferguson[5], A. M. Koekemoer[5], M. Giavalisco[6], and B. Mobasher[7]

ABSTRACT

The observed deficit of strongly Lyman-α emitting galaxies at $z > 6.5$ is attributed to either increasing neutral hydrogen in the intergalactic medium (IGM) and/or to the evolving galaxy properties. To investigate this, we have performed very deep near-IR spectroscopy of $z \gtrsim 7$ galaxies using MOSFIRE on the Keck-I Telescope. We measure the Lyman-α fraction at $z \sim 8$ using two methods. First, we derived $N_{\rm Ly\alpha}/N_{\rm tot}$ directly using extensive simulations to correct for incompleteness. Second, we used a Bayesian formalism (introduced by Treu et al. 2012) that compares the $z > 7$ galaxy spectra to models of the Lyman-α equivalent width ($W_{\rm Ly\alpha}$) distribution at $z \sim 6$. We explored two simple evolutionary scenarios: pure *number evolution* where Lyman-α is blocked in some fraction of galaxies (perhaps due to the IGM being opaque along only some fraction of sightlines) and uniform *dimming evolution* where Lyman-α is attenuated in all galaxies by a constant factor (perhaps owing to processes from galaxy evolution or a slowly increasing IGM opacity). The Bayesian formalism places stronger constraints compared with the direct method. Combining our data with that in the literature we find that at $z \sim 8$ the Lyman-α fraction has dropped by a factor >3 (84% confidence interval) using both the dimming and number evolution scenarios, compared to the $z \sim 6$ values. Furthermore, we find a tentative "positive" Bayesian evidence favoring the number evolution scenario over dimming evolution, extending trends observed at $z \lesssim 7$ to higher redshift. Comparison of our results with theoretical models imply the IGM volume averaged neutral hydrogen fraction $\gtrsim 0.3$ suggesting that we are likely witnessing reionization in progress at $z \sim 8$.

1. INTRODUCTION

With growing number of spectroscopically confirmed galaxies at $z > 6.5$, it is evident that there is a dearth of galaxies with high rest-frame Lyman-α equivalent widths ($W_{\rm Ly\alpha}$). We illustrate this problem in Figure 1, showing the observed $W_{\rm Ly\alpha}$ for galaxies with high spectroscopic confidence at $z > 6.5$ (Iye et al. 2006; Ouchi et al. 2010; Rhoads et al. 2012; Finkelstein et al. 2013; Pentericci et al. 2014). The lack of high-$W_{\rm Ly\alpha}$ galaxies is unlikely due to selection bias as these galaxies span a wide range of continuum magnitudes (lower panels in Figure 1) i.e., we are not just limited to some brighter UV continuum galaxies causing the observed decline in $W_{\rm Ly\alpha}$. A similar trend is also observed in the Lyman-α fraction of continuum-selected Lyman-break galaxies: while the fraction of Lyman-α galaxies increases from $z = 3$ to 6 (Stark et al. 2011), there is a marked decline at $z > 7$ (Fontana et al. 2010; Robertson et al. 2010; Vanzella et al. 2011; Ono et al. 2012; Schenker et al. 2012; Caruana et al. 2012; Treu et al. 2013; Pentericci et al. 2014; Faisst et al. 2014; Schenker et al. 2014).

Clearly something is changing in the Lyman-α emitting population at $z \gtrsim 7$. As Lyman-α emission is sensitive to neutral hydrogen fraction in the intergalactic medium (IGM: McQuinn et al. 2007), it is tempting to associate the decline in the Lyman-α fraction with an increasing neutral hydrogen fraction in the IGM, as inferred from QSO sightlines at these redshifts (Fan et al. 2006) because there is no indication that the galaxy properties contributing to $W_{\rm Ly\alpha}$ are evolving rapidly. For example, at $3 < z < 6$ (Ouchi et al. 2008; Stark et al. 2011; Mallery et al. 2012; Zheng et al. 2014), where the IGM is mostly ionized (Fan et al. 2002), there is no observed evolution in the $W_{\rm Ly\alpha}$ distribution and this offers insight into the galaxies' physical processes. Also, there is no evolution in the number density of Lyman-α emitting galaxies in this redshift range (Kashikawa et al. 2006; Iye et al. 2006; Dawson et al. 2007; Ouchi et al. 2008). Clearly, if it were known that the (intrinsic) $W_{\rm Ly\alpha}$ distribution at $3 < z < 6$ continues to higher redshift, then the observed decline in $W_{\rm Ly\alpha}$ at $z > 7$ must stem from an increasing neutral hydrogen fraction in the IGM. For example, Konno et al. (2014) recently reported a marked decline in the number density of Lyman-α-emitting population at $z \sim 7.3$ from narrow-band imaging, consistent with a declining $W_{\rm Ly\alpha}$.

The declining $W_{\rm Ly\alpha}$ distribution could suggest an increasing neutral hydrogen fraction with redshift. This is consistent with recent theoretical studies (e.g., Forero-Romero et al. 2012) that the observed decline in the Lyman-α fraction at $z \sim 7$ requires about $\sim$

[1] George P. and Cynthia Woods Mitchell Institute for Fundamental Physics and Astronomy, and Department of Physics and Astronomy, Texas A&M University, College Station, TX. 77845
[2] Department of Astronomy, The University of Texas at Austin, Austin, TX. 78712
[3] Department of Statistics, Texas A&M, College Station, TX. 77845
[4] National Optical Astronomy Observatory, Tuscon, AZ. 85719
[5] Space Telescope Science Institute, Baltimore, MD. 21218
[6] Department of Astronomy, University of Massachusetts, Amherst, MA. 01003
[7] Department of Physics and Astronomy, University of California, Riverside, CA. 92521

[*] The data presented herein were obtained at the W.M. Keck Observatory, which is operated as a scientific partnership among the California Institute of Technology, the University of California and the National Aeronautics and Space Administration. The Observatory was made possible by the generous financial support of the W.M. Keck Foundation.

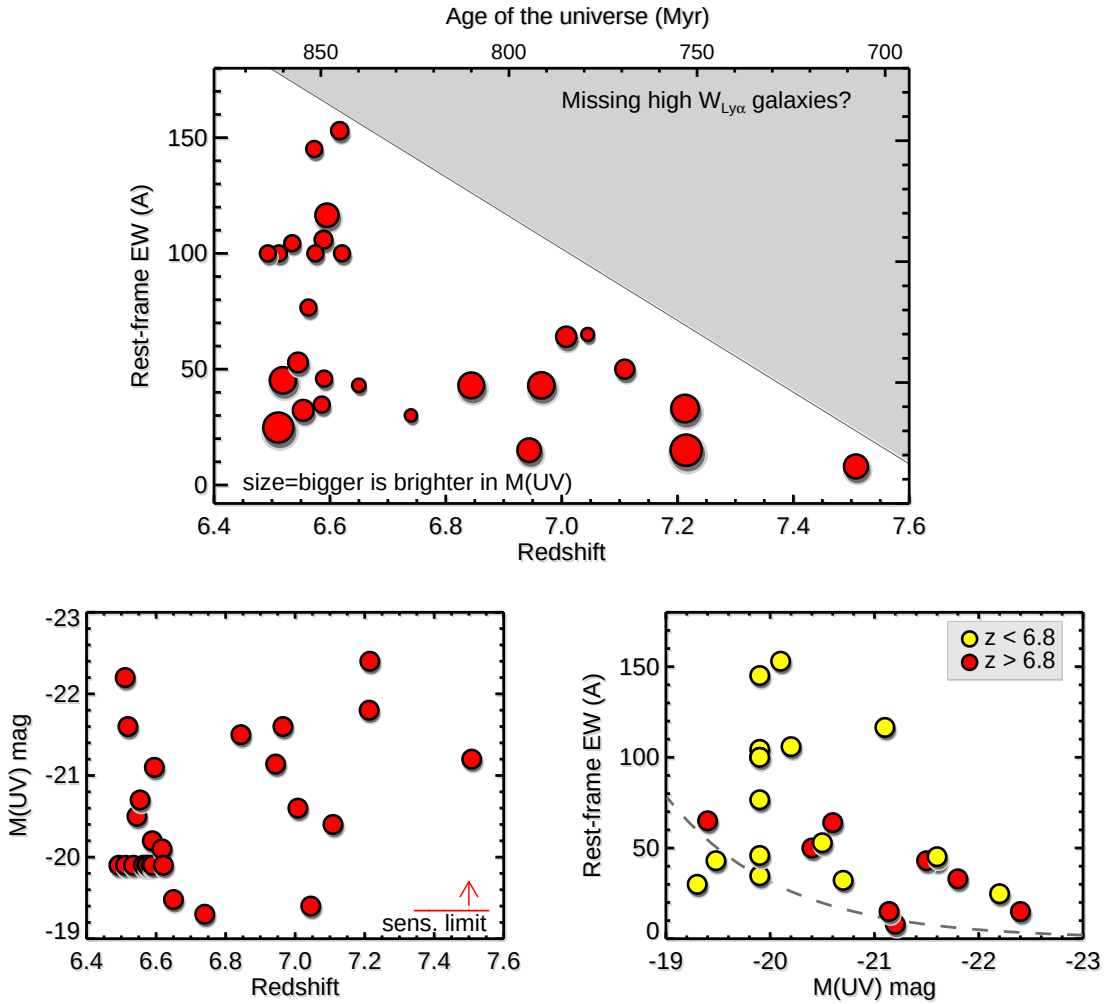

FIG. 1.— **Missing high Lyman-α equivalent width galaxies** –Top panel: Redshift evolution of rest-frame Lyman-α equivalent width ($W_{\rm Ly\alpha}$) for galaxies with high spectroscopic confidence (Iye et al. 2006; Ouchi et al. 2010; Schenker et al. 2012; Vanzella et al. 2011; Ono et al. 2012; Rhoads et al. 2012; Finkelstein et al. 2013; Pentericci et al. 2014). There is a missing population of high $W_{\rm Ly\alpha}$ galaxies at $z \gtrsim 7$. This deficit is not due to selection bias or observing galaxies with only brighter continuum magnitudes (lower left panel) as these galaxies span a wide range of M_{UV} magnitudes. The clustering of galaxies at M_{UV}=-20 is due to the survey limit. Bottom-right panel shows that the galaxies at $z < 6.8$ as well as $z > 6.8$ span a similar range of M_{UV} magnitudes. The dashed line shows a typical $z \gtrsim 7$ spectroscopic survey limit, assuming a Lyman-α line flux limit 5×10^{-18}erg s^{-1}cm^{-2}; Treu et al (2013), Finkelstein et al (2013) : current spectroscopic surveys at $z > 7$ are sensitive to galaxies with $W_{\rm Ly\alpha}$ greater than this threshold.

$10-20\%$ neutral hydrogen, when combined with field-to-field variance (Taylor & Lidz 2014), a possibly evolving escape fraction of ionizing photons (Dijkstra et al. 2014), and/or incidence of Lyman-α absorption systems (Bolton & Haehnelt 2013). If reionization is in fact extremely rapid, with the neutral fraction evolving from $>10\%$ to $< 0.01\%$ in the $\lesssim$200 Myr from $z \sim 7$ and $z \sim 6$, then one would indeed expect a strong evolution in the number of Lyman-α galaxies formed in this short redshift range (Jensen et al. 2013).

On the other hand, the evolution in Lyman-α emission may signify evolution in the physical properties of galaxies at $z > 6$. And indeed, some recent works at $z > 7$ show some evolution in galaxy's physical properties. Galaxies at $z > 7$ have bluer colors (Bouwens et al. 2010; Labbé et al. 2010; Wilkins et al. 2011; Finkelstein et al. 2012; Tilvi et al. 2013, but see also McLure 2011, Dunlop et al 2012), likely due to lower dust extinction, (e.g., Finkelstein et al. 2012), with lower stellar mass (Finkelstein et al. 2010; Schaerer & de Barros 2010), and smaller sizes (Malhotra et al. 2012; Ono et al. 2013). However, these results, if anything, should support the idea that the decline in $W_{\rm Ly\alpha}$ and Lyman-α fraction is caused by the increasing neutral hydrogen fraction; lesser dust and smaller masses would make it easier for Lyman-α photons to escape unless it is a result of gas accretion (Kereš et al. 2009) with high covering fraction (but see also Jones et al. 2013). Indeed, this may be the case as empirical arguments suggest that the gas accretion rate exceeds the star-formation rate at $z \gg 4$ (Papovich et al. 2011). Therefore, there are plausible reasons to suspect that any evolution in the UV

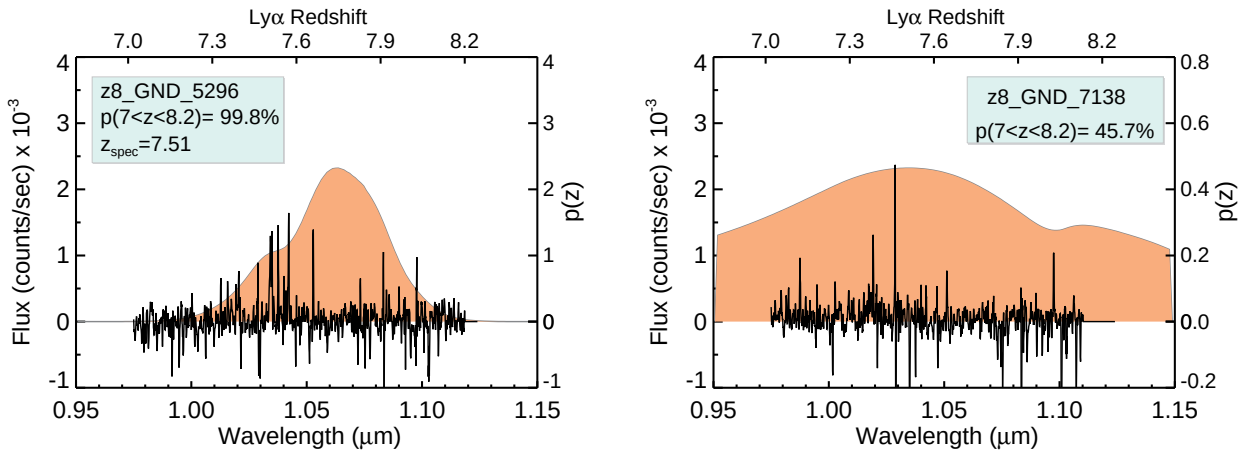

FIG. 2.— MOSFIRE Y-band spectra of two galaxies, representative of our sample. The shaded region shows the photometric probability density $p(z)$ for each galaxy. The left panel shows the object that was spectroscopically confirmed with Lyman-α line detection at $z = 7.51$ (Finkelstein et al. 2013), with a narrow $p(z)$. The right panel shows an object with no line detection, and a broad $p(z)$. While deriving the Lyman-α fraction, we use all available information in the 1D spectra, as well as correcting our analysis for $p(z)$ outside of our observed spectroscopic wavelength range.

continuum properties of LBGs at $\gtrsim 7$ might also contribute to the evolution in $W_{\rm Ly\alpha}$(e.g., Finkelstein et al. 2012; Lorenzoni et al. 2013; Bouwens et al. 2014).

In this paper, we measure the redshift evolution of Lyman-α emission at $z > 7$ and we study the nature of the evolution of $W_{\rm Ly\alpha}$ using simple empirical models. In addition to using our deep spectroscopic observations (Finkelstein et al. 2013), to increase the sample size in order to mitigate the effects of cosmic (field-to-field) variance (Tilvi et al. 2009) and increase the significance from independent datasets, we also combine our data with observations from the literature (Treu et al. 2013). We measure the evolution of the Lyman-α fraction (the fraction of galaxies with $W_{\rm Ly\alpha}$ above a certain limit) using both a direct measurement of $N_{\rm Ly\alpha}/N_{\rm tot}$ (§3.1), and testing the $z > 7$ $W_{\rm Ly\alpha}$ distribution against that at $z \sim 6$ using a Bayesian formalism against an empirical model (§ 3.2; Treu et al. 2012, 2013). In §4 and §5 we discuss our results and present a summary of our findings, respectively. Where applicable, we assume cosmological parameters $\Omega_M = 0.27$, $\Omega_\Lambda = 0.73$, and $H_0 = 71$ km s^{-1} Mpc^{-1}.

2. CANDIDATE SELECTION AND SPECTROSCOPIC OBSERVATIONS

To select $z \gtrsim 7$ candidate galaxies for spectroscopic follow-up we used extremely deep WFC3/F160W-selected and PSF-matched photometric catalog (Finkelstein et al. 2013) created using imaging from the Cosmic Assembly Near-infrared Deep Extragalactic Legacy Survey (CANDELS: Grogin et al. 2011; Koekemoer et al. 2011). All candidates were selected using photometric redshifts, derived using the photometric redshift code EAZY (Brammer et al. 2008) which uses redshifted spectral energy distribution templates and compare them with the observed multi-band photometry for a given galaxy. In addition to deriving the best-fit photometric redshift, it provides the photometric redshift probability density $p(z)$ for each object. In the following analyses we make use of full photometric redshift distribution instead of just the best-fit redshifts. Each object in our sample was required to have $> 70\%$ of the integral of $p(z)$ in the primary peak and $> 25\%$ at $z = 7.5 - 8.5$ for the $z \sim 8$ sample and at $z = 6.5 - 7.5$ for the $z \sim 7$ sample, and be detected in both F125W and F160W bands at S/N$>$ 3.5. For further details about the candidate selection and data reduction and calibration, we direct the reader to Finkelstein et al. (2013).

We targeted nine $z \sim 8$ and 34 $z \sim 7$ candidate galaxies using Multi-object Spectrometer For Infra-Red Exploration (MOSFIRE: McLean et al. 2012), a near-IR multi-object spectrograph on the Keck Telescope, from Apr 17-18, 2013. The $z \sim 8$ selection of objects to be put on MOSFIRE masks were prioritized based on their magnitude and the amount of their $p(z)$ contained within the redshift range $7 < z < 8.2$, covered by the MOSFIRE Y-band.

In this study, we focus on nine $z \sim 8$ galaxies that have spectroscopic observations. The spectroscopic observing conditions were excellent with median seeing FWHM$\simeq 0\farcs7$. We used the MOSFIRE data reduction pipeline to reduce the raw data and extract 2D, wavelength calibrated spectra. To flux calibrate the 1D spectra, we used the standard star measurements taken during the same observing nights. We found that the flux errors in the reduced 1D spectra are overestimated. In order to correct these errors, we used the ratio of standard deviation of flux and median value of flux errors for a given spectrum, and scaled the flux errors such that this ratio is close to unity (as was done in Finkelstein et al. 2013). These corrected flux errors are consistent with the MOSFIRE exposure time calculator. The typical exposure time per galaxy is about 5–6 hours which allowed us to reach deep line flux sensitivity of $\simeq 2 \times 10^{-18}$ erg s^{-1} cm^{-2} (5σ: although this limit varies with wavelength and the presence of sky emission features).

Our MOSFIRE observations used the Y-band filter covering 0.97-1.12 μmm, sensitive to Lyman-α emission from galaxies at $7 < z < 8.2$. Figure 2 shows spectra of two galaxies typical of our sample, along with their photometric redshift probability densities, $p(z)$. The galaxy in the left panel of Figure 2 has a narrow $p(z)$ with

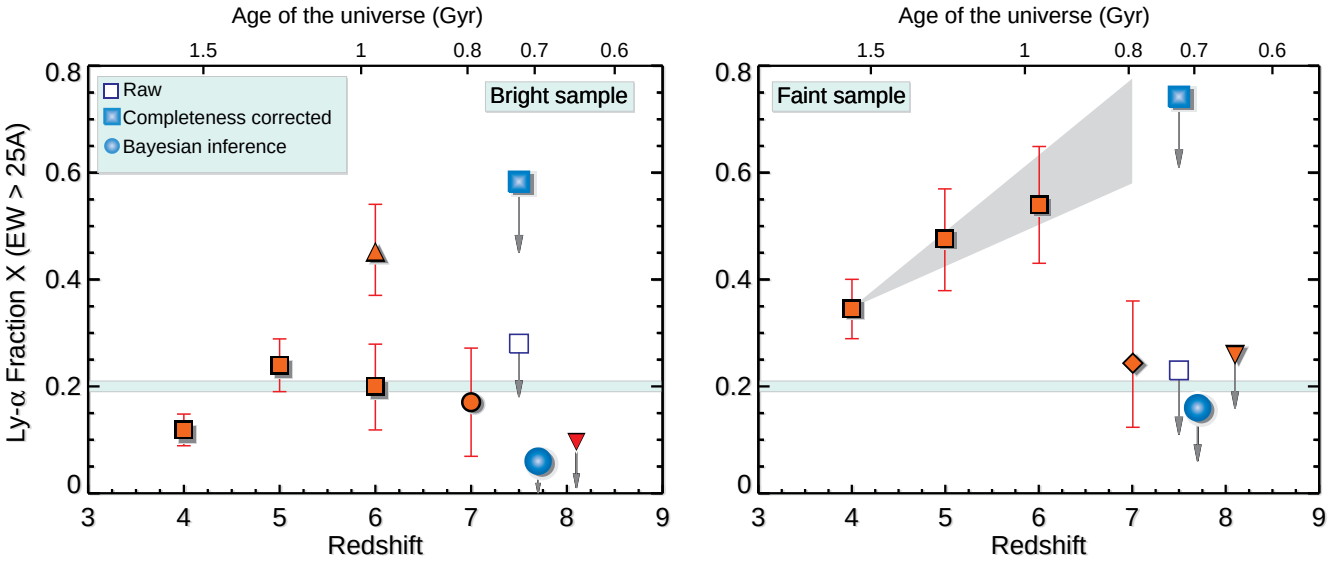

FIG. 3.— Redshift evolution of the Lyman-α fraction with $W_{\rm Ly\alpha} > 25$ Å. The left and right panels show results for brighter ($M_{\rm UV} < -20.25$) and fainter sample ($M_{\rm UV} > -20.25$), respectively. The blue open square indicates the uncorrected limit (for our data only; 84% confidence) on the fraction from the direct method (§ 3.1) while the filled square shows the limit including completeness corrections and accounting for the photometric redshift distributions. The filled blue circle shows the Lyman-α fraction derived using the Bayesian formalism (§ 3.2). Red filled squares, upward-pointing triangle, and downward-pointing triangles are data from (Stark et al. 2011; Curtis-Lake et al. 2012; Ono et al. 2012), respectively. The filled diamond is the combined data taken from Ono et al. (2012) which is composed of data from (Fontana et al. 2010; Pentericci et al. 2011; Schenker et al. 2012). There is a difference in the Lyman-α fraction estimated from the direct method and Bayesian method which stems from using our data only and using the combined data (with Treu et al 2013), respectively. But the unique advantage of using the Bayesian inference is that the results at $z \sim 8$ are *relative* to the $z \sim 6$ distribution. If the drop in the Lyman-α fraction is due to increasing neutral hydrogen fraction in the IGM, this occurs over a short, <300 Myr, period, and we are likely witnessing reionization in progress at $z > 7$.

$\mathcal{P}_z \equiv \int_{z=7.0}^{z=8.2} p(z)\, dz = 99.8\%$, while the galaxy in the right panel has a broad $p(z)$ with $\mathcal{P}_z = 45.7\%$.

3. REDSHIFT EVOLUTION OF LYMAN-α FRACTION

3.1. *Direct Measure*

The most straightforward measure of the Lyman-α fraction is the ratio of number of galaxies with Lyman-α emission to the total number of galaxies observed. Figure 3 shows the redshift evolution of Lyman-α fraction with $W_{\rm Ly\alpha} > 25$ Å. Formally, none of the objects in our sample are detected with $W_{\rm Ly\alpha}$ greater than this value and so our measurements of the fraction are upper limits. The open blue squares show the raw Lyman-α fraction obtained from our deep MOSFIRE observations, $X = N_{Ly\alpha}/N_{tot} < 0.28$ (84% confidence derived from Poisson statistics for 0/4 objects with EW>25Å) for the brighter ($M_{\rm UV} < -20.25$ mag) sample and $X < 0.23$ (84% confidence for 0/5 objects) for the fainter sample ($M_{\rm UV} > -20.25$ mag).

The raw fractions above must be corrected for the wavelength dependent sensitivity of the observed spectra. To estimate this correction, we performed extensive simulations, similar to those described in Stark et al. (2011). First, we inserted artificial sources at random positions along the dispersion direction in the reduced 2D spectra. We then recover the sources using the same automated method as for the real data: extracting one-dimensional spectra, fitting a Gaussian profile to significant lines and then compute the S/N from the fit. Emission features with S/N > 5 are considered "recovered". The completeness $C_i'(m, W, z)$ for an object is then

$$C_i'(m_i, W_i, z) = {\rm N_{rec}}/{\rm N_{ins}}, \qquad (1)$$

where $\rm N_{ins}$ and $\rm N_{rec}$ are the number of simulated (inserted) and recovered artificial sources in the 2D spectra at a given apparent magnitude, m_i, with Lyman-α equivalent width W_i, and redshift z.

We must modify the completeness function to account for $p(z)$, because there is a probability of Lyman-α falling outside the wavelength range covered by the Y-band filter for some objects, and thus

$$C_i(m_i, W_i) = \int_{z=7}^{z=8.2} C_i'(m_i, W_i, z)\, p(z)\, dz \qquad (2)$$

The effective completeness for all objects with equivalent width W and absolute magnitude M (M=$m - \mu$, where μ is the distance modulus and m is the observed F125W magnitude) is then

$$C_{\rm eff}(M, W) = \sum_{i=1}^{N} C_i(m_i, W_i)/N, \qquad (3)$$

where N is the total number of galaxies in the given (brighter or fainter) sample. The Lyman-α fraction corrected for incompleteness is then $X_{\rm corr} = X/C_{\rm eff}$.

In Figure 3 filled squares show the completeness corrected Lyman-α fraction. The completeness corrected fraction is $X_{\rm corr} < 0.58$ for the brighter subsample, and <0.74 for the fainter sample. For our sample, this is primarily a consequence of the fact that the $p(z)$ is not entirely covered by the MOSFIRE Y-band observations. On average $\langle \mathcal{P}_z \rangle = 0.45$, and this has the effect of nearly doubling the Lyman-α fraction. For this reason, in the

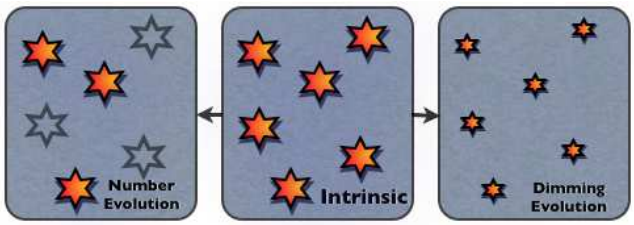

FIG. 4.— A cartoon representation of our two evolutionary models– number evolution versus dimming evolution used in the Bayesian implementation. In the number evolution scenario only some fraction of Lyman-α emitting galaxies are visible either due to transparent sight lines or other physical processes while in the dimming evolution model, Lyman-α photons from all galaxies are equally attenuated, say e.g., due to homogeneous distribution of neutral hydrogen in the IGM. In reality, the observed distribution is likely to be a combination of both scenarios.

following sections, we explore an alternative method to measure X.

3.2. *Bayesian Inference*

We use a Bayesian formalism developed by Treu et al. (2012) to measure the evolution of the Lyman-α equivalent width distribution from $z \sim 6$ to $z > 7$. This method constrains the Lyman-α equivalent width distribution based on all available information; detections, non-detections, wavelength-dependent line-flux sensitivity, and incomplete wavelength coverage (similar to the Direct method with completeness simulations, §3.1). An advantage of this formalism is that the results obtained from different data sets or instruments can be combined together easily by simply multiplying the posterior probabilities, and that the probability at $z > 7$ is *relative* to the $z \sim 6$ distribution; any change in $z \sim 6$ equivalent width distribution will change the $z > 7$ values accordingly.

Following Treu et al. (2012), we use the observed $z \sim 6$ $W_{\rm Ly\alpha}$ (Stark et al. 2011) distribution function, $p_6(W_{\rm Ly\alpha})$, modeled as the combination of a Gaussian and a delta function,

$$p_6(W) = \frac{2A}{\sqrt{2\pi}W_c} \exp\left(-\frac{W^2}{2W_c^2}\right) H(W) + (1-A)\delta(W), \quad (4)$$

where we use the shorthand $W \equiv W_{\rm Ly\alpha}$, $W_c = 47$ Å, and A is the fraction of Lyman-α emitters, taken as $A = 0.38$ for $M_{\rm uv} < -20.25$ and $A = 0.89$ for $M_{\rm UV} > -20.25$. H is the Heaviside step function and $\delta(x)$ is the Delta-function.

The physics of the evolution of Lyman-α emission is likely very complex, and could involve physical processes associated with the galaxies that depend on redshift, galaxy mass, inclination angle, etc., and a highly inhomogeneous (patchy) IGM with rapidly evolving opacity (see below). Here, we model the evolution of the probability distribution $p(W)$ at $z > 6$ under two simple empirical cases, as in Treu et al. (2012). These two models do not involve any reionization physics but merely represent how the observed equivalent width distribution at $z > 6$ compares with $z \sim 6$ distribution. The first limiting-case is a *number evolution* scenario where only some fraction, ϵ_{ne}, of Lyman-α galaxies are either completely absorbed or do not emit Lyman-α at all, while the remaining $1-\epsilon_{ne}$ are unattenuated, $p_{ne}(W) = \epsilon_{ne}P_6(W) + (1-\epsilon_{ne})\delta(W)$. The second limiting-case is a uniform *dimming evolution* model which could correspond to either evolution in galaxy properties or a slowly (and homogeneously) evolving IGM neutral fraction (see Fig. 4). Parametrically, the dimming model assumes that Lyman-α emission from all galaxies at $z > 6$ is attenuated by the same factor, ϵ_{de}, such that $p_{de}(W) = p_6(W/\epsilon_{de})/\epsilon_{de}$. Our number evolution and dimming evolution models bracket the range of possible physical effects from reionization and galaxy-evolution physics. For example, Jensen et al. (2014, see their Figure 11) and Mesinger et al. (2014) show that patchy reionization may prefer a scenario more similar to our dimming-evolution model. Regardless, the observed equivalent width distribution of Lyman-α in galaxies is likely a combination of both scenarios. These two models are identical in parametrization to the *patchy* and *smooth* models of Treu et al. (2012). However, we avoid using the latter nomenclature in order to avoid confusion with the theoretical models that include physics of reionization.

While these two models are simplistic, they span the full empirical range of evolution in Lyman-α emission, which allows us to test if the data provide any evidence for the form of the empirical evolution. Reionization is expected to be a highly patchy process based on theoretical expectations (e.g., Furlanetto et al. 2004; Iliev et al. 2006; Zahn et al. 2007; Mesinger & Furlanetto 2008; Finlator et al. 2009). If the evolution of the Lyman-alpha emission is a result of such rapid reionization, then we would expect the data to favor the number evolution model. If on the other hand, the data favors the dimming evolution model, then some other process (or a combination of processes) may be responsible. Therefore, the two models discussed above provide a starting point for understanding if there is evidence that the evolution in the Lyman-α emission from galaxies favors "number" evolution versus "dimming" evolution. Furthermore, these models have the advantage that their effects on the Lyman-α distribution function can be solved analytically, and therefore straightforward to test against observations. The models can also be easily adapted as more data, both at $z < 7$ and at $z > 7$, become available.

3.2.1. *Implementation*

We now describe how the above models can be applied to the observations. For an observed spectrum of a galaxy, the observables are the apparent magnitude m, the flux density f_i and variance σ_i at each pixel i corresponding to each wavelength, λ_i, from the spectroscopic data. Following the methodology in Treu et al. (2012, 2013), each wavelength in the spectrum has some likelihood of containing a Lyman-α emission line with redshift $z_i = \lambda_i/(1216\ \text{Å}) - 1$, and equivalent width W. For an unresolved line, we model the distribution function of the line flux density as a Gaussian given by

$$p(f_i, m|W, z_j) = \frac{1}{\sqrt{2\pi}\sigma_i} e^{-\frac{1}{2}\left(\frac{f_i - W f_m}{\sigma_i}\right)^2} \quad (5)$$

where $f_m \equiv f_0\ 10^{-0.4m}\ c\lambda_0^{-2}(1+z)^{-1}$, $f_0 = 3.631 \times 10^{-20}$ erg s^{-1} Hz^{-1} cm^{-2}. For a resolved line we replace $W f_m$ in equation 5 with the line flux distributed as a Gaussian with $\sigma_\lambda = 1$ Å (equation 5 in Treu et

al. 2012). In the region (pixels) where there is no emission line contribution ($W = 0$), $p(f_i, m|W, z_j)$ is simply a normal distribution with mean f_i and variance σ_i^2. The likelihood of the dataset, $\{f\}$, given a particular combination of these parameters is then $p(\{f\}, m|\epsilon, z_j) = \int\ [\prod_i\ p(f_i, m|\epsilon, z_j)] \times p(W|\epsilon)\ dW$.

By Bayes' theorem, the posterior probability on ϵ is then simply the product

$$p(\epsilon, z_j|\{f\}, m) = \frac{p(\{f\}, m|\epsilon, z_j) \times p(\epsilon) \times p(z_j)}{Z}, \quad (6)$$

where this equation is valid for both $\epsilon = \epsilon_s$ and ϵ_p. We adopt a uniform prior $p(\epsilon)$ between 0 and 1 for both cases, where a value of $\epsilon = 1$ would imply no evolution. The prior on $p(z_j)$ is the photometric redshift probability density for each galaxy. Because $p(\{f\}|\epsilon, z_j, m)$ depends on the S/N ratio of the data, it contains the wavelength-dependent sensitivity function. The normalization is Z=$\prod [p(\{f\}, m|\epsilon) \times p(\epsilon)\ \times\ p(z_j)]$. Intuitively, smaller values of Z imply that there is less likelihood that the model describes the data. The ratio of this factor between two models (number evolution versus dimming evolution) can be used as an evidence in favor of one model over the other (e.g., Kass & Raftery 1995). For the simple models used here, equation 6 can be solved analytically (Treu et al. 2012).

3.2.2. *Results*

We applied this Bayesian formalism to the spectra of nine galaxies at $z \sim 8$. In the following we derive the results using these nine spectra as well as combining this sample with that of Treu et al. (2013). Combining our sample of nine galaxies with Treu et al. (2013), nearly doubles the current spectroscopic sample at $z \sim 8$.

Figure 5 shows the posterior probability densities derived from nine $z \sim 8$ spectra in our sample, combined with the posteriors taken from Treu et al. (2013). The 84% confidence intervals on ϵ are derived by integrating the posterior. For our data alone, we obtain $\epsilon_{ne} < 0.56$ and $\epsilon_{de} < 0.74$ at $z \sim 8$ for the number evolution and dimming evolution models respectively. If we combine these results with those of Treu et al. (2013), we obtain $\epsilon_{ne} < 0.30$ and $\epsilon_{de} < 0.25$, for the number evolution and dimming evolution models respectively.

The normalization of the posteriors allow us to derive the Bayesian evidence between the two models (e.g., Jeffreys 1961; Kass & Raftery 1995)[9]. For our data alone, we find a tentative "positive" Bayesian evidence favoring the number evolution model, with $2\ln(Z_{ne}/Z_{de}) = 2.5$. This evidence drops slightly but remains positive towards the number evolution model with $2\ln(Z_{ne}/Z_{de}) = 2.2$ when we combine our data with that from Treu et al. (2013). Therefore the evidence is minimally significant that the evolution in the $W_{\rm Ly\alpha}$ distribution at $z \sim 8$ favors the number evolution model.

Qualitatively, the reason the Bayesian evidence favors number evolution of the $W_{\rm Ly\alpha}$ distribution is that even the relatively small sample sizes are becoming large enough to discriminate between these simple evolutionary models. For example, under the dimming evolution model, the $W_{\rm Ly\alpha}$ distribution shifts such that there are relatively many objects with low $W_{\rm Ly\alpha}$ and fewer objects with high Lyman-α, while the total number of objects with Lyman-α emission remains unchanged (assuming one can detect the lower levels of Lyman-α emission). If the true evolution follows the dimming evolution model, then we would expect more Lyman-α detections at low $W_{\rm Ly\alpha}$, which is not observed and is therefore less favored by the Bayesian analysis. In contrast, in the number evolution model, some fraction of Lyman-α sources are blocked, keeping the relative distribution of Lyman-α unchanged, and is favored by the current data. Clearly larger sample will be needed to confirm these results and/or increase the evidence against the dimming evolution model.

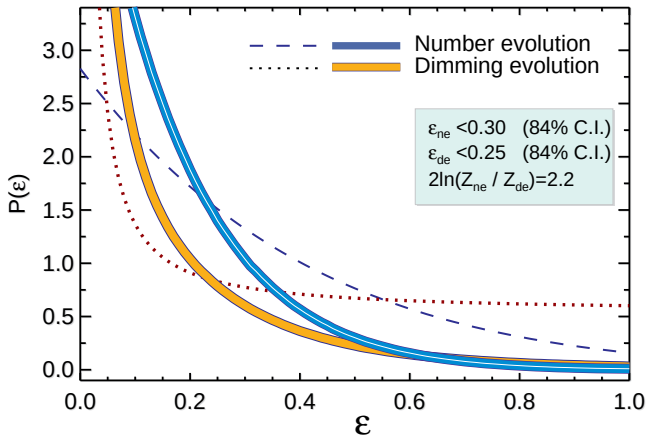

FIG. 5.— Posterior probability density of ϵ where ϵ is the proportionality factor between Lyman-α fraction $X_{z\sim8}$ and $X_{z\sim6}$. Blue and orange lines show the probability using the combined sample (This work + Treu et al 2013), for number evolution and dimming evolution models, respectively. Also labeled are the 84% value for both models. Dashed and dotted lines represent probability density using our dataset alone. The data provide "positive" evidence ($2\ln(Z_p/Z_s) = 2.2$) in favor of the number evolution model over the dimming evolution model using the significance scale of Kass & Raftery (1995).

The posterior distribution of ϵ is broader for our sample compared to that of Treu et al. (2013), because we detect Lyman-α in one object (Finkelstein et al. 2013) and have three other marginal detections ($\simeq 2-3\sigma$). In addition, our MOSFIRE Y-band observations did not fully cover $p(z)$ of all nine galaxies. Thus, there is a finite probability that the Lyman-α line could lie outside the Y-band, which again broadens the ϵ distribution.

4. DISCUSSION

Based on the ϵ constraints above, and fitting functions used for $z \sim 6$ equivalent width distributions, the Lyman-α fraction in the number evolution model is $X_{z\sim8} = \epsilon_p X_{z\sim6}$, while in the dimming evolution case $X_{z\sim8} = {\rm erfc}(W/\sqrt{2}\epsilon_s W_c)/\ {\rm erfc}(W/\sqrt{2}W_c) X_{z\sim6}$ where *erfc* is the complimentary error function.

For our dataset alone, the Lyman-α fraction $X_{\rm z\sim8} < 0.56 X_{\rm z\sim6}$ and $X_{\rm z\sim8} < 0.79 X_{\rm z\sim6}$ (all 84% confidence limits) for number evolution and dimming evolution models respectively. For the combined data (with Treu et al 2013), $X_{\rm z\sim8} < 0.30 X_{\rm z=6}$ and $X_{\rm z\sim8} < 0.05 X_{\rm z=6}$ for

[9] Kass & Raftery (1995) define the significance scale in favor of one model over the other using the Bayes factors Z_1 and Z_2 as $S = 2\ln(Z_1/Z_2)$, with S=0 − 2 (not worth more than a bare mention), S=2 − 6 (positive), S=6 − 10 (strong), S> 10 (very strong).

TABLE 1
Results of using different $z \sim 6$ equivalent distributions for our data alone.

Reference	Distribution type	Sources used	$\epsilon(W>25$Å$)$		Lyman-α fraction ($W>25$Å) relative to $z\sim6$		Evidence ratio[a]
			ϵ_{ne}	ϵ_{de}	X_{ne}	X_{de}	
St11	Truncated gaussian plus a delta function $W_{Ly\alpha}>0$Å	$z\sim6$ Stark+11, Treu+14	<0.56	<0.74	<0.56	<0.79	2.5 (2.2[b])
P11	Same as St11 but with tail extending at $W_{Ly\alpha}>100$Å	$z\sim6$ Pentericci+11, Treu+12	<0.58	<0.75	<0.58	<0.80	2.3
Sc14	Log-normal like with negative tail extending at $W_{Ly\alpha}<-20$Å	$3<z<6.5$ as in Schenker et al 2014	<0.59	<0.80	<0.59	<0.86	2.4
T14[c]	Same as in Sc14 but with negative tail extending at $W_{Ly\alpha}<-50$Å	–	<0.59	<0.81	<0.59	<0.86	2.3
W150[c]	Same as P11 but with large number of sources with $W_{Ly\alpha}>150$Å	–	<0.28	<0.18	<0.28	<0.02	6.1

These values are for our data only. All limits are 84% confidence interval.
[a] Bayesian evidence ratio $2\ln(Z_{ne}/Z_{de})$ derived from our dataset alone; see also footnote 9.
[b] The value in parenthesis denotes the Bayesian evidence after combining the posterior for our samples with those of Treu et al. (2013).
[c] This work.

number evolution and dimming evolution models respectively. In Figure 3 we show the constraints from the number evolution model only (as this is the conservative limit) as filled blue circles. For the brighter sample, $X_{z\sim8}<0.06$ and $X_{z\sim8}<0.01$ while for the fainter sample $X_{z\sim8}<0.16$ and $X_{z\sim8}<0.03$ for number evolution and dimming evolution models respectively. The implication is that at $z>7$, the fraction of Lyman-α emitters is reduced by a factor of >3 (84% confidence interval) compared to the fraction at $z\sim6$. At the 95% confidence interval, the Lyman-α decline at $z>7$ is >2, implying a strong evolution even at this more conservative limit.

4.1. *Effect of Using Different $z\sim6$ Distributions*

Our results show that there is strong evidence for evolution in the Lyman-α equivalent width distribution. The nature of this evolution however depends on the assumed $z=6$ equivalent width distribution (Stark et al. 2011). Here we test other possible $z=6$ Lyman-α equivalent width distributions to see how this choice affects our conclusions.

To test this effect, Treu et al. (2012) explored $z\sim6$ equivalent width distribution with a tail extending towards larger equivalent width objects, similar to Pentericci et al. (2011), for fainter sample. They find that this equivalent width distribution does not alter their conclusions. We performed a similar test on our data using $z\sim6$ equivalent width distribution with a uniform tail extending towards higher$-W_{Ly\alpha}$ (150Å) objects. Using this equivalent width distribution, the Bayesian probabilities change only slightly with ϵ_{ne} changing from $\epsilon_{ne}<0.56$ to $\epsilon_{ne}<0.58$ and ϵ_{de} increases from $\epsilon_{de}<0.74$ to $\epsilon_{de}<0.75$ for our data.

In addition, we explored two more $z\sim6$ equivalent width distributions: 1) similar to the log-normal distribution used in Schenker et al. (2014) with additional tail extending towards negative equivalent widths ($W_{Ly\alpha}<-20$Å) and 2) an extreme distribution with negative tail extending to $W_{Ly\alpha}<-50$Å. We show these distributions in Figure 6 and tabulate the results of these tests in Table 1, using our data alone as the results for these distributions are not available from Treu et al. (2013). Thus, it can be seen that our results do not change significantly if the input $z\sim6$ distribution includes a significant tail extending to very negative equivalent widths. However, if the $z\sim6$ Lyman-α distribution is significantly different, for example the one similar to the dotted line (W150) shown in Figure 6, then the derived constraints would be significantly different. The W150 distribution which contains large number of galaxies with high $W_{Ly\alpha}>150$Å yields $X_{z\sim8}<0.28X_{z=6}$ for the number evolution model, much lower compared to the other input equivalent width distributions. Thus, it is important to have a much larger spectroscopic sample

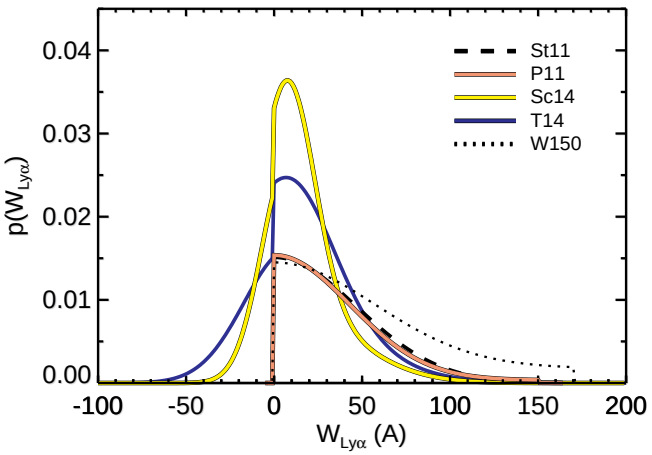

Fig. 6.— Different $z\sim6$ Lyman-α equivalent width distributions used to test their effect on our results. Legends indicate different distributions described in Table 1. The dotted line (W150) is an arbitrary distribution chosen to demonstrate how different the $z\sim6$ equivalent distribution needs to be in order to significantly change the Lyman-α fraction evolution from the current value. This distribution yields much lower Lyman-α fraction with $X_{z\sim8}<0.28X_{z=6}$ for the number evolution model.

of $z \gtrsim 6$ galaxies in order to construct a robust equivalent width distribution at this redshift.

4.2. *Physical Interpretation*

There are a few possible reasons that can explain the observed sharp decline in the $W_{\rm Ly\alpha}$. It may be the samples are biased: we may be preferentially targeting only bright continuum galaxies with lower $W_{\rm Ly\alpha}$. However, this is unlikely because Figure 1 shows that the galaxies with Lyman-α span a wide range of $M_{\rm UV}$ and that UV continuum limits of $z \gtrsim 7$ surveys are nearly same as that of $z < 7$ surveys. It may also be that the $z > 7$ samples include a larger number of lower-z contaminants. We think this is unlikely because it does not explain the steep decline in the $W_{\rm Ly\alpha}$ values (top panel in Figure 1) in spectroscopically detected galaxies at $z > 6.5$,

It may be evolution in the intrinsic galaxy properties that is responsible. Previous work has shown that galaxies at $z > 6$ have lower dust extinction (e.g., Finkelstein et al. 2012), smaller sizes and lower stellar mass, making it easier for Lyman-α photons to escape. Robertson et al. (2010) also find evolution in the UV continuum properties of galaxies, and discuss how this may contribute to the decline in the $W_{\rm Ly\alpha}$ in spectroscopic samples. Galaxies at $z > 7$ may also have higher gas accretion rates relative to their SFRs than lower redshift galaxies (e.g., Papovich et al. 2011; Finkelstein et al. 2012), which could suppress the escape of Lyman-α photons depending on the gas dynamics (infall velocity versus outflow rates) or if the covering fraction of the infalling gas is large. On the other hand, recent work (e.g., Iwata et al. 2009) implies that the Lyman-continuum photon escape fraction should be *higher* at $z > 3$ than at lower redshift to account for reionization, but see also Boutsia et al. (2011) where they find a low continuum escape fraction in Lyman-break selected galaxies at $z = 3.3$.

While some evolution of the physical properties of $z > 7$ galaxies occurs, it seems galaxy evolution alone is unable to account for the decline in the Lyman-α distribution. Rather, the most plausible explanation is that both a changing neutral hydrogen fraction in the IGM and evolution from galaxy properties contribute to the decline in the $W_{\rm Ly\alpha}$ distribution. Based on our results, the fraction of galaxies with strong Lyman-α equivalent widths has dropped significantly from $z \sim 6.5$ to $z > 7$. If this suppression in Lyman-α emission is solely due to the IGM evolution, it can be directly interpreted as an increase in the optical depth, $\Delta\tau_{\rm Ly\alpha}$, from $z = 6.5$ to $z = 7.5$, where $\langle \exp(-\Delta\tau_{\rm Ly\alpha}) \rangle = \epsilon$ (for both the number and dimming evolutionary models). Based on our results, in a simplistic case where reionization is uniform, the conservative limit on the optical depth of $\Delta\tau_{Ly\alpha} > 1.2$ (84% confidence interval) at $z \sim 7.5$. This is similar to the rapid evolution in the opacity of the Gunn & Peterson (1965) trough, where the extrapolated relation from Fan et al. (2006) predicts $\Delta\tau = (1 + z_{7.5})/(1 + z_6)^{4.3} = 2.3$.

The observed rapid decline in the Lyman-α fraction is consistent with recent theoretical predictions. However, these studies suggest that at $z \sim 7$ we need only $\sim 10 - 20\%$ neutral hydrogen fraction to explain the observed Lyman-α fraction decline if we account for cosmic variance, evolving escape fraction of ionizing photons and increasing incidence of optically thick absorption systems (Bolton & Haehnelt 2013; Taylor & Lidz 2014; Dijkstra et al. 2014). Mesinger et al. (2014) argue based on their model that, at 68% confidence, the decline in the Lyman-α fraction at $z \sim 7$ from lower redshift can not be greater than a factor of two unless galaxy evolution processes also contribute to the decline in Lyman-α photons. However, at 95% confidence the observed decline in Lyman-α may stem solely from the evolution of the IGM in their model. At $z > 7$, however, it is possible that there is in fact a more rapid increase in the neutral hydrogen fraction which may explain the steep observed decline of Lyman-α equivalent widths of individual galaxies (see §4.3 below). To investigate and minimize these observational uncertainties, we therefore need much larger spectroscopic samples of $z > 7$ galaxies.

In addition to the declining Lyman-α fraction, our simplistic models show first tentative evidence towards number evolution scenario at $z > 7$, extending recent results seen at $z \lesssim 7$ (Pentericci et al. 2014). Therefore, the data support the idea that some process related to decreasing high $W_{\rm Ly\alpha}$ galaxies is dominant. This is consistent with reionization where regions are opaque, likely due to neutral hydrogen, blocking a fraction of sightlines while leaving others unaffected. This makes the prediction that if we survey enough area, we should find objects with high $W_{\rm Ly\alpha}$, but they should be rare. Indeed, there is a recent report of a weak detection ($\sim 4\sigma$) of a galaxy at $z = 7.6$ with $W_{\rm Ly\alpha} = 160$Å (Schenker et al. 2014), which if confirmed could further support our interpretation.

4.3. *Implications for Reionization*

Several theoretical studies using semi-analytical and numerical simulations have developed models of IGM evolution and its effect on the observations (e.g., Miralda-Escudé et al. 2000; Ciardi et al. 2006; Gnedin & Fan 2006; Furlanetto & Pritchard 2006; McQuinn et al. 2007; Mesinger & Furlanetto 2008; Choudhury et al. 2009; Crociani et al. 2011; Dijkstra et al. 2011; Alvarez & Abel 2012; Jensen et al. 2013). In this section, to estimate the neutral hydrogen fraction $f_{\rm HI}$ at $z \sim 8$, we use two different models which predict the probability of Lyman-α equivalent widths given certain neutral hydrogen fraction in the IGM combined with line-of-sight Lyman-α absorbers (Bolton & Haehnelt 2013) and models that include evolving escape fraction of ionizing photons (Dijkstra et al. 2014).

Figure 7 shows the cumulative probability distribution of Lyman-α equivalent widths comparing our results with the theoretical predictions from Bolton & Haehnelt (2013) and Dijkstra et al. (2014) for the fainter sample. Our results are shown only for the number evolution model. The Cyan-filled region shows model predictions at $z \sim 7$ from Bolton & Haehnelt (2013) for a range of Lyman-α velocity offsets from 200 to 600 km s^{-1}, photo-ionization rate $\log(\Gamma_{\rm HI}/S^{-1}) = -14$, and volume average neutral hydrogen fraction of $f_{\rm HI} \sim 0.1$. The yellow-filled region shows the model prediction at $z \sim 8$ (Dijkstra et al. 2014) for $f_{\rm HI} \sim 0.3$ and escape fraction of ionizing photons $< f_{esc} >= 0.04[(1 + z)/5]^4$. Compared

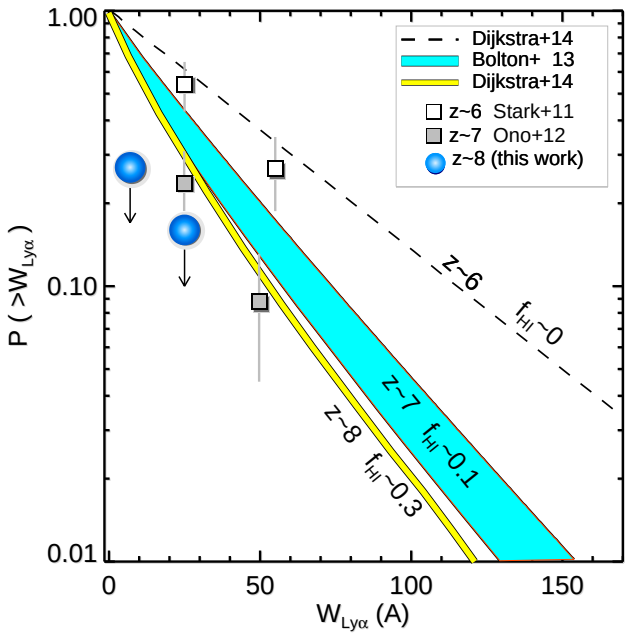

FIG. 7.— Cumulative Lyman-α probability distribution for the faint sample ($M_{UV} > -20.25$ mag) and comparison of model predictions (Bolton & Haehnelt 2013; Dijkstra et al. 2014) to estimate the neutral hydrogen fraction in the IGM at $z \sim 8$. Dashed line shows the reference $z \sim 6$ Lyman-α EW distribution used in the models, equivalent to a neutral hydrogen fraction $f_{\rm HI} \sim 0$ while open squares represent $z \sim 6$ observations from (Stark et al. 2011), used in our Bayesian models. Cyan-filled regions shows model predictions at $z \sim 7$ for a volume averaged $f_{\rm HI} \sim 0.1$ (Bolton et al 2014). Filled Gray squares are the observations from (Ono et al. 2012, and references there in). The yellow-filled region shows the model prediction at $z \sim 8$ (Dijkstra et al. 2014) for $f_{\rm HI} \sim 0.3$. Our results, shown in filled blue circles (shown only for the number evolution scenario) are significantly lower compared with the model predictions. This implies that the volume-averaged neutral hydrogen fraction at $z \sim 8$ is at least $f_{\rm HI} \gtrsim 0.3$.

with these model predictions, our current Lyman-α emitter fraction are lower by a factor of ~ 2. Thus, we conclude that the neutral hydrogen fraction at $z \sim 8$ is $f_{\rm HI} \gtrsim 0.3$ considering the evolution of neutral hydrogen fraction as well as evolving galaxy properties such as winds, ionizing escape fraction, etc. If the decline is solely due to the reionization, the amount of neutral hydrogen fraction at $z \sim 8$ will be much higher because the model predictions (Bolton & Haehnelt 2013; Dijkstra et al. 2014) in Figure 7 already include some galaxy evolution. This is consistent with inferences of the neutral hydrogen fraction based on the evolution of the UV and Lyman-α luminosity functions (Robertson et al. 2013; Konno et al. 2014), and thus, the reionization of the universe is likely in progress at $z \sim 8$.

5. SUMMARY

We investigated the evolution of the Lyman-α fraction from $z \sim 6$ to $z \sim 8$ using extremely deep spectroscopic observations of nine galaxies, obtained using the MOSFIRE Y-band that covers the redshift range $7 < z < 8.2$. We explored two different methods to study the Lyman-α fraction : a direct method with extensive completeness simulations to account for the incompleteness and a Bayesian inference method using two simplistic models– number evolution versus dimming evolution.

The Bayesian method yields much stronger constraints than the direct method due to its 'relative' inference– the Lyman-α fraction at $z \sim 8$ is relative to the $z \sim 6$ values and any change in $z \sim 6$ values will change the derived $z \sim 8$ values accordingly. Combining our data with that of Treu et al. (2013), we found that the Lyman-α fraction at $z \sim 8$ has dropped significantly, by a factor of >3 (84% confidence), compared with $z \sim 6$ values. However, it may be that the other factors such as (rapid) evolution in galaxy properties, or field-to-field variations also affect the Lyman-α emission distribution.

Our results show a tentative "positive" evidence towards the number evolution model with Bayesian evidence ratio of $2\ln(Z_{ne}/Z_{de}) = 2.2$ extending earlier $z \sim 7$ results to higher redshift, $z > 7$. Furthermore, comparing our results with theoretical predictions, we find that the neutral hydrogen fraction $f_{\rm HI}$ at $z \sim 8$ is $\gtrsim 0.3$. To corroborate these results further, and understand how the Lyman-α width distribution function evolves from $z = 6$ to $z > 7$, we need larger samples of galaxies (particularly with high $W_{\rm Ly\alpha}$). Only with that knowledge can we constrain the nature of reionization.

We thank Tommaso Treu and Kasper Schmidt for useful conversations and comments on the manuscript. We also thank James Rhoads and Sangeeta Malhotra for helpful comments and suggestions. The authors also thank the referee for a careful reading, and for comments and suggestions that improved the quality and clarity of this work. The authors wish to recognize and acknowledge the very significant cultural role and reverence that the summit of Mauna Kea has always had within the indigenous Hawaiian community. We are most fortunate to have the opportunity to conduct observations from this mountain. We also thank the CANDELS team for providing a valuable dataset. This work is supported by HST program GO-12060, provided by NASA through a grant from the STScI, which is operated by the AURA.

REFERENCES

Alvarez, M. A., & Abel, T. 2012, ApJ, 747, 126
Bolton, J. S., & Haehnelt, M. G. 2013, MNRAS, 429, 1695
Boutsia, K., Grazian, A., Giallongo, E., et al. 2011, ApJ, 736, 41
Bouwens, R. J., Illingworth, G. D., Oesch, P. A., et al. 2010, ApJ, 708, L69
Bouwens, R. J., Illingworth, G. D., Oesch, P. A., et al. 2014, arXiv:1403.4295
Brammer, G. B., van Dokkum, P. G., & Coppi, P. 2008, ApJ, 686, 1503
Caruana, J., Bunker, A. J., Wilkins, S. M., et al. 2012, MNRAS, 427, 3055
Choudhury, T. R., Haehnelt, M. G., & Regan, J. 2009, MNRAS, 394, 960
Ciardi, B., Scannapieco, E., Stoehr, F., et al. 2006, MNRAS, 366, 689
Crociani, D., Mesinger, A., Moscardini, L., & Furlanetto, S. 2011, MNRAS, 411, 289
Curtis-Lake, E., McLure, R. J., Pearce, H. J., et al. 2012, MNRAS, 422, 1425
Dijkstra, M., Mesinger, A., & Wyithe, J. S. B. 2011, MNRAS, 414, 2139
Dijkstra, M., Wyithe, S., Haiman, Z., Mesinger, A., & Pentericci, L. 2014, arXiv:1401.7676

Dawson, S., Rhoads, J. E., Malhotra, S., et al. 2007, ApJ, 671, 1227
Dunlop, J. S., McLure, R. J., Robertson, B. E., et al. 2012, MNRAS, 420, 901
Fan, X., Narayanan, V. K., Strauss, M. A., et al. 2002, AJ, 123, 1247
Fan, X., Carilli, C. L., & Keating, B. 2006, ARA&A, 44, 415
Faisst, A. L., Capak, P., Carollo, C. M., Scarlata, C., & Scoville, N. 2014, arXiv:1402.3604
Finkelstein, S. L., Papovich, C., Dickinson, M., et al. 2013, Nature, 502, 524
Finkelstein, S. L., Papovich, C., Salmon, B., et al. 2012, ApJ, 756, 164
Finkelstein, S. L., Papovich, C., Giavalisco, M., et al. 2010, ApJ, 719, 1250
Finlator, K., Özel, F., Davé, R., & Oppenheimer, B. D. 2009, MNRAS, 400, 1049
Fontana, A., Vanzella, E., Pentericci, L., et al. 2010, ApJ, 725, L205
Furlanetto, S. R., Hernquist, L., & Zaldarriaga, M. 2004, MNRAS, 354, 695
Furlanetto, S. R., & Pritchard, J. R. 2006, MNRAS, 372, 1093
Forero-Romero, J. E., Yepes, G., Gottlöber, S., & Prada, F. 2012, MNRAS, 419, 952
Gnedin, N. Y., & Fan, X. 2006, ApJ, 648, 1
Grogin, N. A., Kocevski, D. D., Faber, S. M., et al. 2011, ApJS, 197, 35
Gunn, J. E., & Peterson, B. A. 1965, ApJ, 142, 1633
Iliev, I. T., Mellema, G., Pen, U.-L., et al. 2006, MNRAS, 369, 1625
Iwata, I., Inoue, A. K., Matsuda, Y., et al. 2009, ApJ, 692, 1287
Iye, M., Ota, K., Kashikawa, N., et al. 2006, Nature, 443, 186
Jeffreys, H. 1961, 3rd ed. Oxford Univ. Press. MR0187257
Jensen, H., Laursen, P., Mellema, G., et al. 2013, MNRAS, 428, 1366
Jensen, H., Hayes, M., Iliev, I., et al. 2014, arXiv:1406.1358
Jiang, L., Bian, F., Fan, X., et al. 2013, ApJ, 771, L6
Jones, T. A., Ellis, R. S., Schenker, M. A., & Stark, D. P. 2013, ApJ, 779, 52
Kashikawa, N., Shimasaku, K., Malkan, M. A., et al. 2006, ApJ, 648, 7
Kereš, D., Katz, N., Fardal, M., Davé, R., & Weinberg, D. H. 2009, MNRAS, 395, 160
Kass, E. R. and Raftery, E. A. 1995, JASA, 90, 430
Koekemoer, A. M., Faber, S. M., Ferguson, H. C., et al. 2011, ApJS, 197, 36
Konno, A., Ouchi, M., Ono, Y., et al. 2014, arXiv:1404.6066
Labbé, I., González, V., Bouwens, R. J., et al. 2010, ApJ, 716, L103
Lorenzoni, S., Bunker, A. J., Wilkins, S. M., et al. 2013, MNRAS, 429, 150
Malhotra, S., Rhoads, J. E., Finkelstein, S. L., et al. 2012, ApJ, 750, L36
Mallery, R. P., Mobasher, B., Capak, P., et al. 2012, ApJ, 760, 128
McLean, I. S., Steidel, C. C., Epps, H. W., et al. 2012, Proc. SPIE, 8446,
McLure, R. J., Dunlop, J. S., de Ravel, L., et al. 2011, MNRAS, 418, 2074
McQuinn, M., Hernquist, L., Zaldarriaga, M., & Dutta, S. 2007, MNRAS, 381, 75
Mesinger, A., & Furlanetto, S. R. 2008, MNRAS, 386, 1990
Mesinger, A., Aykutalp, A., Vanzella, E., et al. 2014, arXiv:1406.6373
Miralda-Escudé, J., Haehnelt, M., & Rees, M. J. 2000, ApJ, 530, 1
Ono, Y., Ouchi, M., Mobasher, B., et al. 2012, ApJ, 744, 83
Ono, Y., Ouchi, M., Curtis-Lake, E., et al. 2013, ApJ, 777, 155
Oesch, P. A., Bouwens, R. J., Illingworth, G. D., et al. 2013, ApJ, 773, 75
Ouchi, M., Shimasaku, K., Akiyama, M., et al. 2008, ApJS, 176, 301
Ouchi, M., Shimasaku, K., Furusawa, H., et al. 2010, ApJ, 723, 869
Papovich, C., Finkelstein, S. L., Ferguson, H. C., Lotz, J. M., & Giavalisco, M. 2011, MNRAS, 412, 1123
Pentericci, L., Fontana, A., Vanzella, E., et al. 2011, ApJ, 743, 132
Pentericci, L., Vanzella, E., Fontana, A., et al. 2014, arXiv:1403.5466
Rhoads, J. E., Hibon, P., Malhotra, S., Cooper, M., & Weiner, B. 2012, ApJ, 752, L28
Robertson, B. E., Furlanetto, S. R., Schneider, E., et al. 2013, ApJ, 768, 71
Robertson, B. E., Ellis, R. S., Dunlop, J. S., McLure, R. J., & Stark, D. P. 2010, Nature, 468, 49
Schaerer, D., & de Barros, S. 2010, A&A, 515, A73
Schenker, M. A., Stark, D. P., Ellis, R. S., et al. 2012, ApJ, 744, 179
Schenker, M. A., Ellis, R. S., Konidaris, N. P., & Stark, D. P. 2014, arXiv:1404.4632
Stark, D. P., Ellis, R. S., & Ouchi, M. 2011, ApJ, 728, L2
Taylor, J., & Lidz, A. 2014, MNRAS, 437, 2542
Treu, T., Trenti, M., Stiavelli, M., Auger, M. W., & Bradley, L. D. 2012, ApJ, 747, 27
Treu, T., Schmidt, K. B., Trenti, M., Bradley, L. D., & Stiavelli, M. 2013, ApJ, 775, L29
Tilvi, V., Papovich, C., Tran, K.-V. H., et al. 2013, ApJ, 768, 56
Tilvi, V., Malhotra, S., Rhoads, J. E., et al. 2009, ApJ, 704, 724
Vanzella, E., Pentericci, L., Fontana, A., et al. 2011, ApJ, 730, L35
Wilkins, S. M., Bunker, A. J., Stanway, E., Lorenzoni, S., & Caruana, J. 2011, MNRAS, 417, 717
Zahn, O., Lidz, A., McQuinn, M., et al. 2007, ApJ, 654, 12
Zheng, Z.-Y., Wang, J.-X., Malhotra, S., et al. 2014, MNRAS, 199